Adsorption (2009) 15: 247–253
DOI 10.1007/s10450-009-9184-7

Studies on mesoporous niobosilicates synthesized using F127 triblock copolymer

Agnieszka Feliczak-Guzik · Agata Wawrzynczak · Izabela Nowak

Published online: 17 April 2009

Abstract A detailed characterization of cage-like mesoporous SBA-16 niobosilicate with tailored features of the structure is reported. The materials were synthesized in a $EO_{106}PO_{70}EO_{106}$(F127)-water system under acidic conditions and the pore diameters were tuned by varying the hydrothermal treatment temperature and time. The effects of the synthesis parameters on the structural/textural properties of the cubic Im3m niobosilicates have been investigated systematically. We show that the total pore volume, pore diameter, and micro-/mesopores ratio can be controlled very efficiently by changing the synthesis parameters.

Keywords NbSBA-16 · Cage-like structure · Characterization · Structural/textural properties · Niobium source

1 Introduction

The discovery of supramolecular(surfactant)-templated ordered mesoporous materials (OMMs) provides an extension of ordered microporous structures of zeolites and zeotypes into the mesopore range. Initially discovered MCM-41 and MCM-48 (Kresge et al. 1992) as well as many other important ordered mesoporous materials, such as HMS, KIT-1, SBA-3, and SBA-15 exhibit channel-like pore structures (e.g., Bagshaw et al. 1995). The succeeding discovery of ordered silica with cage-like mesoporous structures is a further major achievement and breakthrough in the synthesis of mesoporous materials (e.g., Zhao et al. 1998a; Huo et al. 1994). Many efforts have been taken to characterize their cavity connection, as well as tailor their structures for various applications. The use of commercially available surfactants of the poly(ethylene oxide)-poly(propylene oxide)-poly(ethylene oxide) $EO_XPO_yEO_X$ type, i.e., inexpensive and environmentally friendly nonionic triblock copolymer in the formation of mesoporous materials was reported (Zhao et al. 1998b) in the late 1990s. The synthesis carried out with these surfactants usually occurs in very low pH ($pH \ll 2$) solutions where the interaction proceeds through an $S^0H^+X^-I^+$ mechanism (S^0H^+ being the surfactant in interaction with a hydronium ion, X^- the chloride ion and I^+ the protonated silica). This results in SBA- and FDU-type materials. Among polymer-templated OMMs with channel-like (SBA-3, -12, -15) and cage-like (SBA-1, -6, -16 and FDU-1) mesopores, the cage-like materials become especially popular because of their attractive 3-dimensional mesoporous structures, which facilitate mass transfer and are less prone for pore blockage. These features of cage-like materials make them attractive for adsorption, catalysis and separations as well as for immobilization of biomolecules, sensors and catalysts.

Among the most intensively studied non-ionic surfactants or triblock copolymers templates used for the synthesis of OMMs is the F127 copolymer, which is a poly(ethylene oxide)-poly(propylene oxide)-poly(ethylene oxide)—$EO_{106}PO_{70}EO_{106}$—triblock copolymer (Zhao et al. 1998b). The large surface area of OMMs created by using the F127 copolymer, known as SBA-16, was essential for improvement of gas adsorption properties of surface photo voltage (SPV) devices (Yamada et al. 2002). SBA-16 is a material with a 3D cubic arrangement of mesopores correspond-

Honoring Professor Mietek Jaroniec, on the occasion of his 60th birthday.

A. Feliczak-Guzik · A. Wawrzynczak · I. Nowak (✉)
Adam Mickiewicz University, Faculty of Chemistry,
Grunwaldzka 6, 60-780 Poznan, Poland
e-mail: nowakiza@amu.edu.pl

ing to the Im3m space group. Each mesopore, i.e., cage in this body-centered-cubic (bcc) structure is connected with its eight nearest neighbors (small apertures) to form a multidirectional system of mesoporous network, as proven by high-resolution electron microscopy (Sakamoto et al. 2000). Furthermore, SBA-16, and other SBA's as well, possess a substantial amount of micropores (Ryoo et al. 2001) (up to 50% of its volume) originating from the more hydrophilic EO chains of the surfactant which penetrate the amorphous siliceous walls during synthesis (Kruk et al. 2000; Ryoo et al. 2000; Imperor-Clerc et al. 2000). This dual porosity system makes the SBA materials excellent candidates for adsorption and catalysis, sensors and nanoreactors. Other requirements for such systems include good accessibility of pores, which can be achieved by creating a 3D porous structure.

To date the SBA-16 materials (Yu et al. 2000, 2001; Van Der Voort et al. 2002; Cheng et al. 2003, 2004; Wang et al. 2004; Kim et al. 2004; Kleitz et al. 2004; Grudzien et al. 2006, 2007; Fulvio et al. 2007) have been synthesized mostly by employing Pluronic F127. In most cases, the existing recipes afforded SBA-16 with relatively small pore sizes and quite low pore volumes. Additionally, the control over the morphology of SBA materials can be obtained by variations in the synthesis parameters, or through the use of co-solvents, co-surfactants or various salts. Here we demonstrate a simple and effective method for the synthesis of niobium containing SBA-16 materials by using of two different procedures in order to diverge the textural properties. It is worthy to stress that mesoporous niobosilicates are promising materials for a wide range of industrial applications, including gas separation, catalysis, water waste management, etc. (Nowak et al. 2002, 2003; Nowak and Ziolek 2005).

2 Experimental section

2.1 Synthesis of materials

SBA-16 and NbSBA-16 were hydrothermally synthesized by using F127 ($EO_{106}PO_{70}EO_{106}$, BASF) as a structure-directing agent and tetraethylorthosilane (TEOS, 99% Aldrich) as a silica source. In a typical synthesis (after Van Der Voort et al. 2002; Kim et al. 2004), 4 g of F127 was dissolved in 30 g of deionized water and 120 g of HCl (2M) at 30 °C. A chosen amount of TEOS and ammonium complex of trisoxalate niobium(V) (CBMM, Brazil) were added to the solution. The starting molar composition was: 1 TEOS : 0.0156 Nb source : 0.0075 F127 : 5.7 HCl : 193 H_2O and such composition is going to be denoted as method A. The mixture is maintained at 30 °C for 4 h with vigorous stirring, followed by heating at 80 or 100 °C for different periods (8 or 24 h). The solid products were filtered off and then washed with deionized water repeatedly. After drying at room-temperature overnight, the products were calcined in ambient air for 6 h with a heating rate of 2 °C/min from room temperature up to 550 °C. Additionally, a second procedure—method B—was applied with a starting molar composition of 1.0 TEOS : 0.0156 Nb source : 0.0040 F127 : 4.0 HCl : 130 H_2O for NbSBA-16. Thus, the denotation of samples used in this paper is going to be: NbSBA-16—method name—heating temperature—heating time, e.g., NbSBA-16-A-80-8.

2.2 Characterization

Measurements X-ray diffraction (XRD) patterns were recorded between 0.6 and 40° (2θ) on a Bruker D4Advance diffractometer (Cu K_α radiation; $\lambda = 0.154$ nm) with a step size of 0.02°. The quantitative chemical analysis was performed on Philips MiniPal equipment. Porosity and surface area were determined by using a Micromeritics 2010 automated gas adsorption system using nitrogen as the adsorbate at liquid nitrogen temperature (−196 °C). All samples were outgassed under vacuum for 3 h at 300 °C. Transmission electron micrographs (TEM) measurements were recorded on JEOL 2010 microscope operated at 80 kV. The sample particles were suspended in alcohol and the suspension was deposited on a copper grid coated with a polymer supported film.

Calculation methods The specific surface area (SA) was calculated by the BET method from adsorption data in the relative pressure range from 0.05 to 0.2. The cross-sectional area of nitrogen molecule was assumed to be equal to 0.162 nm^2. The total pore volume (V_t) was obtained from the amount of nitrogen adsorbed at a relative pressure (p/p_0) of 0.99. The total volume of micropores, V_{mi}, and primary mesopores, V_{pme}, was assessed using the α_s plot method (Matos et al. 2002) in the range of α_s from 1.8 to 2.2, i.e., from the intercept of the linear segment of the α_s plot that follows the capillary condensation step. The standard reduced adsorption α_s is defined as the ratio of the amount adsorbed on a reference adsorbent—LiChrospher Si-1000 (Jaroniec et al. 1999)—at a given relative pressure to the amount adsorbed at a relative pressure of 0.4. The micropore volume was calculated using the α_s method, however in the α_s range from 0.4 to 1.2, i.e., from the intercept of the linear segment below the onset of the capillary condensation. Two different linear regions were observed, one in the α_s range from 0.4 to 0.8 that yields a volume of intrawall micropores (V_{mi}) and another one in the α_s range from 0.9 to 1.2 that yields a sum ($V_{mi} + V_{sme}$), where V_{sme} is the volume of a population of small mesopores.

The pore size distribution was calculated from the adsorption branch of nitrogen adsorption isotherms by using

the KJS (Kruk-Jaroniec-Sayari) method, which employs in the classical BJH (Barret-Joyner-Halenda) algorithm an accurate statistical film thickness and modified Kelvin equation, both verified on the basis of adsorption data for a series of high quality MCM-41 materials (Kruk et al. 1997). The primary mesopore diameter, w, was defined as maximum on the PSD. However, due to the fact that the geometry of primary mesopores of SBA-16 can be approximated by a sphere rather than a cylinder, this method leads to a systematic underestimation of the size of cage-like pores by about 2 nm. Thus, the primary mesopore cage diameter, D_{me}, was also calculated on the basis of the unit-cell size assessed from XRD (a) and pore volumes assessed from gas adsorption data, i.e., V_{p} and V_{mi} from the α_{s} plot according to the following formula (Matos et al. 2002; Ravikovitch and Neimark 2002):

$$D_{\mathrm{me}} = \alpha\left(\frac{6}{\pi}\frac{\varepsilon_{\mathrm{me}}}{\nu}\right)^{\frac{1}{2}}, \quad \text{where } \varepsilon_{\mathrm{me}} = \frac{\rho_V V_{\mathrm{me}}}{1+\rho_V V_\varepsilon}, \tag{1}$$

where ρ_V is the silica density equal to 2.2 g cm^{-3}.

The minimal wall thickness for all samples studied, h, was calculated according to relations provided in Huo et al. (1994)

$$h = \alpha\frac{\sqrt{3}}{2} - D_{\mathrm{me}}. \tag{2}$$

3 Results and discussion

The EDX analyses performed for all samples show that the synthesis conditions used (low pH, the presence of Cl^- anions, etc.) led to four times lower Nb contents (Si/Nb = ~200 instead of 64), indicating that not all niobium is incorporated to the final product. Additionally, X-ray diffraction data at high angles ($2\theta = 10-60°$) did not show any peaks of niobium(V) oxide phase. Moreover, the diffuse-reflectance UV–vis and FTIR measurements (not shown here) confirmed that niobium was incorporated only into the SBA-16 framework positions.

For the determination of the structure and symmetry of materials, XRD patterns and TEM images were analyzed. The XRD patterns shown in Fig. 1 clearly indicate that for both synthesis methods used for the NbSBA-16 materials preparation analogous structures were formed. The lattice type and the symmetry of the mesoporous materials were accurately determined by indexing of XRD reflections and established to belong to bicontinuous cubic-body-centered Im3m structure, thus providing an indication of the Im3m structure of SBA-16. Additionally, the presence of a higher order peaks at $\sqrt{2}$-, $\sqrt{3}$-, $\sqrt{4}$-, $\sqrt{5}$-times the reciprocal lattice spacing of the primary reflection suggests that the ordered regions of the NbSBA-16-B samples exhibit a cubic mesostructure. The products prepared by using method A show a broad XRD peak (Fig. 1A) with low intensity, while NbSBA-16-B products show well-resolved XRD patterns (Fig. 1B). Three well-resolved diffraction peaks of NbSBA-16-B can be clearly assigned to (1 1 0), (2 0 0), and (2 1 1)

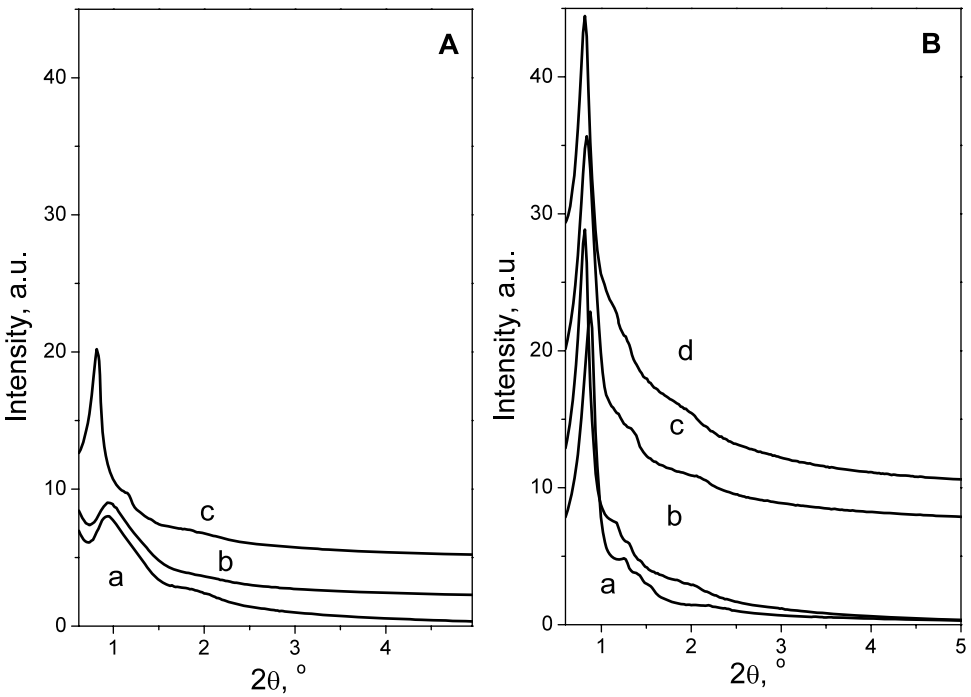

Fig. 1 XRD patterns of NbSBA-16-A (part **A**) and NbSBA-16-B (part **B**) samples: NbSBA-16-A-80-8 (part **A** line a; i.e., Aa), NbSBA-16-A-80-24 (Ab), NbSBA-16-A-100-8 (Ac); NbSBA-16-A-80-8 (Ba), NbSBA-16-A-80-24 (Bb), NbSBA-16-A-100-8 (Bc) and NbSBA-16-A-100-24 (Bd)

Table 1 Textural/structural properties of SBA-16 materials*

Sample	Si/Nb	a, nm	SA, $m^2\ g^{-1}$	V_t, $cm^3\ g^{-1}$	w, nm	D_{me}, nm	h, nm
SiSBA-16-B-80-24	–	15.9	471	0.34	5.8	7.8	5.9
SiSBA-16-B-100-24	–	16.6	706	0.48	6.2	8.5	5.8
NbSBA-16-A-80-24	164	14.1	794	0.95	6.5	7.9	4.4
NbSBA-16-A-100-24	212	15.3	955	0.83	6.5	9.2	4.1
NbSBA-16-B-80-8	226	15.1	508	0.30	5.1	7.2	5.9
NbSBA-16-B-80-24	298	16.2	839	0.53	5.8	9.9	4.1
NbSBA-16-B-100-24	251	16.6	968	0.67	6.5	11.3	2.9

*a—unit-cell size assessed from XRD; SA—specific surface area; V_t—total pore volume; w—primary mesopore diameter from BJH; D_{me} primary mesopore cage diameter, h—minimal wall thickness

diffractions for the cubic space group (Im3m, Q229), respectively. Increasing synthesis temperature yielded in a better XRD pattern resolution and a higher intensity of the reflections owing to the higher particle dispersion and ordering. It is well known, that with a F127/TEOS molar ratio around 0.005 and a temperature ~95 °C a perfect morphology is obtained (Mesa et al. 2005). Moreover, an "amorphous" SBA-16 type mesoporous silica particles (continuous spheres) are produced when the F127/TEOS molar ratio becomes rather low (e.g., 0.002) or rather high (>0.008). Thus, in our case the preparation of organized mesoporous NbSBA-16 with a surfactant as pore structure template has been possible for method B only (see afterward in the text) .

For each sample the values of the unit cell, a, were calculated from visible XRD peaks and the average value was calculated and listed in Table 1. The use of two different synthesis methods yields products with unit cell parameters from 14.0 to 16.6 nm (see Table 1 in which pure siliceous analogues are also tabulated). The augmentation of the hydrothermal treatment time and temperature caused a pronounced shift towards lower angles, an evidence for the enlargement of the unit cells as a function of temperature and time. The introduction of niobium also produced the unit cell expansion. It is well known for more than decade that the transition metal substitution gave an enlargement of the cubic unit cell as well as an increase in the degree of cross-linking in the mesopore walls, i.e., a decrease of the minimal wall thickness (Zhang and Pinnavaia 1996)

Figure 2 shows TEM images for the samples NbSBA-16-B-80-24 and NbSBA-16-B-100-24. The Im3m space group is therefore reliably identified. Large domains of the highly ordered materials are clearly visible. It is well known that the changes in structural properties could also be confirmed by TEM. Even that it difficult to directly access the mesopore diameter or the pore wall thickness by TEM, it is obvious from Fig. 2 that for sample NbSBA-16-B-80-24 the ratio of

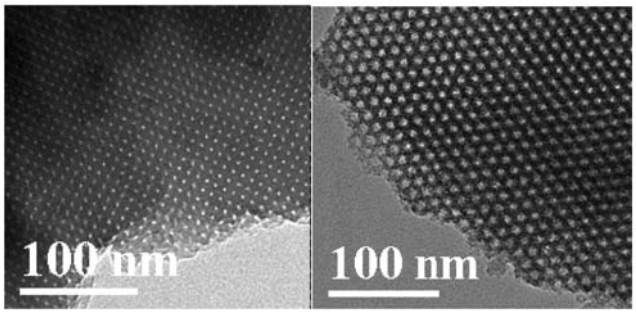

Fig. 2 TEM images of NbSBA-16-B samples synthesized at 80 (*left side*) and 100 °C (*right side*)

void to silica wall volume is lower than for sample NbSBA-16-B-100-24.

The morphology of the SBA-16 samples was determined by the analysis of the SEM micrographs (Fig. 3). The morphology of the NbSBA-16 material was from spherical shape (synthesis no. B, Fig. 3 images A & B) to continuous shapeless and ill-defined one (synthesis no. A, Fig. 3 images C & D). Moreover, the increasing particle size as a function of temperature for the first case can be related to the faster particle growing at higher temperatures resulting in bigger particles for NbSBA-16-B-100-24 than for NbSBA-16-B-80-24.

Nitrogen-physisorption isotherms for the selected niobium containing silicas are presented in Fig. 4. The corresponding parameters for all studied mesoporous materials are given in Table 1. The isotherms show type IV profiles (IUPAC classification), which is typical of mesoporous materials. The hysteresis loop shape (H2) is ascribed to cage-like materials. A steep capillary condensation step is observed for all the NbSBA-16-B samples, suggesting uniform pore dimensions and a good quality ordering of the materials in agreement with the TEM and XRD data. Further-

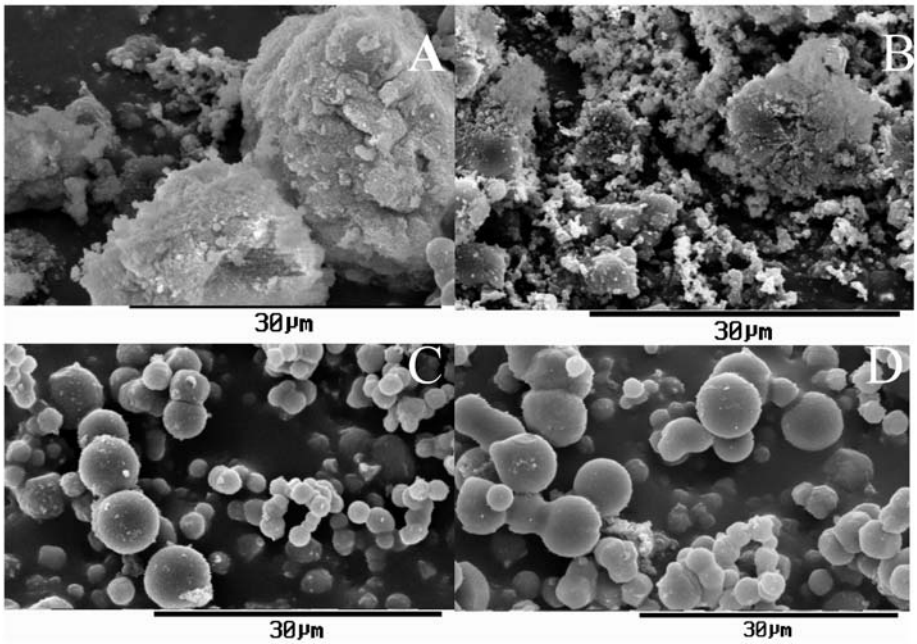

Fig. 3 SEM micrographs for NbSBA-16-A-80-24 (**A**); NbSBA-16-A-100-24 (**B**), NbSBA-16-B-80-24 (**C**) and NbSBA-16-B-100-24 (**D**)

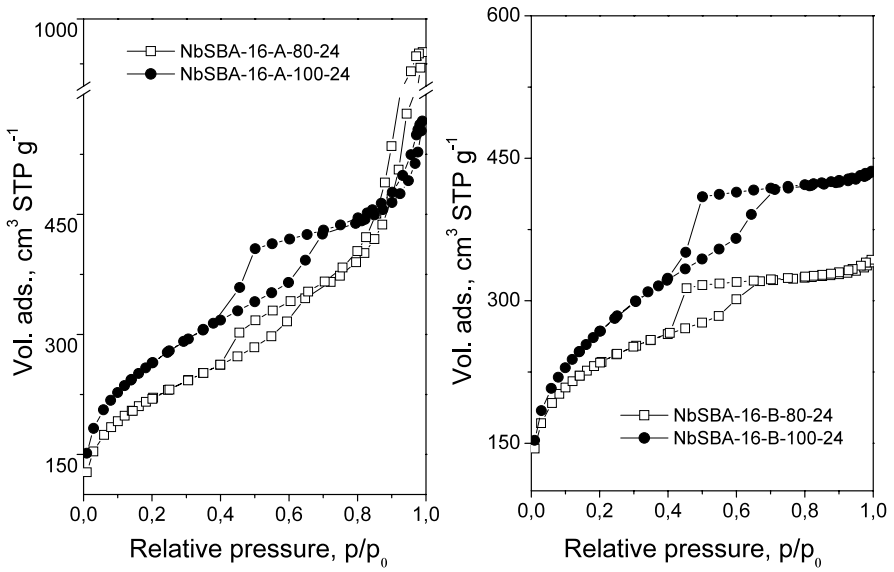

Fig. 4 Nitrogen physisorption isotherms measured at −196 °C on NbSBA-16 samples

more, the capillary condensation appears more pronounced for NbSBA-16-B than for NbSBA-16-A and also with increasing hydrothermal treatment temperature for both series, with NbSBA-16-B-100-24 exhibiting the highest and the most vertical steps. Varying the hydrothermal treatment temperature results in a variation of the total amount of adsorbed nitrogen (estimated at $p/p_0 = 0.98$) and therefore the total pore volume V_t (Table 1). The temperature dependence, in the range investigated in this work, is for most properties beneficial. Sample NbSBA-16-B-80-24 synthesized at low temperature only adsorbs about 0.53 cm^3 liquid nitrogen per gram, whereas in contrast, the sample NbSBA-16-B-100-24 synthesized at higher temperature −0.67 $cm^3\ g^{-1}$.

Pore size distributions determined using the BJH methods established for cylindrical pores are not accurate for materials with cage-like pore structures, i.e., NbSBA-16. However, in order to compare this series the values at maximum of the BJH (w) were therefore reported in Table 1. Also the data obtained from geometrical model (D_{me}) is reported there. Generally, for lower aging temperatures, the total pore volume could be considered as mostly originating from microporosity (<2 nm) with little contribution from the mesopores (cages). As the aging temperature is increased, the contribution of the mesopore volume increases relative, as well as average pore size width, whereas minimal wall thick-

Table 2 Pore volumes of SBA-16 materials*

Sample	V_t, $cm^3\ g^{-1}$	V_{mi}, $cm^3\ g^{-1}$	V_{sme}, $cm^3\ g^{-1}$	V_{pme}, $cm^3\ g^{-1}$	V_{BJH}, $cm^3\ g^{-1}$
SiSBA-16-B-80-24	0.34	0.02	0.08	0.29	0.32
SiSBA-16-B-100-24	0.48	0.02	0.11	0.41	0.46
NbSBA-16-A-80-24	0.95	0.08	0.11	0.76	0.78
NbSBA-16-A-100-24	0.83	0.03	0.18	0.62	0.65
NbSBA-16-B-80-8	0.30	0.05	0.06	0.19	0.27
NbSBA-16-B-80-24	0.53	0.06	0.13	0.34	0.38
NbSBA-16-B-100-24	0.67	0.03	0.21	0.43	0.48

* V_t—total pore volume; V_{mi}—total volume of micropores, V_{pme}—total volume of primary mesopores, V_{sme}—volume of a population of small mesopores; V_{BJH}—mesopore volume estimated using the modified BJH approach

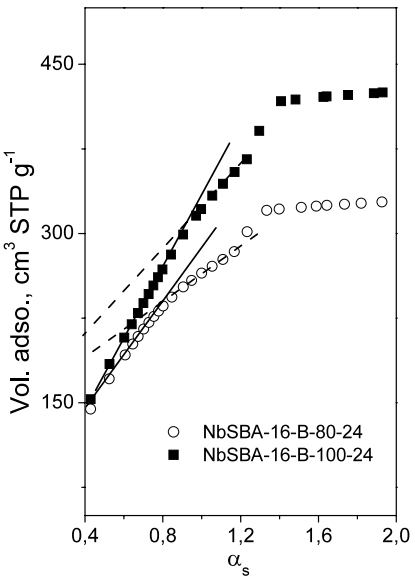

Fig. 5 α_s-plot of selected NbSBA-16-B samples

ness decreases. The same behavior can be observed for the influence of the synthesis time.

Two different linear regions were observed below the capillary condensation step in the α_s-plot (Fig. 5). The low α_s linear region intercept with the ordinate axis yields a volume of micropores (V_{mi}) which is unambiguously ascribed to intrawall micropores. The second linear part intercept yields a sum ($V_{mi} + V_{sme}$) where V_{sme} is the volume of a population of small mesopores. Intrawall small mesopores are generated probably by the coalescence of two micropores specifically starting at temperature of 80 °C (Galarneau et al. 2003). However, one have to keep in mind that in SBA-16 two types of smaller pores exist: (i) ordered small pores which interconnect ordered cages (primary mesopores) and (ii) irregular micropores created by penetration of PEO blocks into silica pore walls, analogous as in SBA-15. Thus, in comparison to SBA-15 cage-like material contains additional ordered interactions, and therefore the amount of complementary pores is larger (Ustinov et al. 2005). The measured values of V_t, V_{mi} and V_{sme} are reported in Table 2. Interestingly, the experimental values of V_{pme} (i.e., calculated as $V_t - V_{mi} - V_{sme}$) are very close to the mesopore volume estimated using the modified BJH approach (V_{BJH}), due to the synthesis temperature higher than mentioned above transition temperature. By varying the hydrothermal temperature and time, materials with a high fraction of intrawall micropores and thick walls (80 °C, 8 h) up to mesoporous materials with few micropores, thinner walls and large primary mesopores (100 °C, 24 h) were obtained.

4 Conclusions

A series of NbSBA-16 materials was prepared with different structural properties focusing on the systematic control of structural/textural parameters. The proper symmetry and the high quality of the samples were established from XRD and TEM measurements. Using the α_s-plot, it was possible to distinguish two different types of intrawall pores. By varying the hydrothermal temperature and time, materials with a high fraction of intrawall micropores and thick wall up to mesoporous materials with few micropores, thinner walls and large primary mesopores can be obtained.

Acknowledgements Izabela Nowak would like to thank Professor Mietek Jaroniec for giving her the opportunity to work in his group at Kent State University (KSU) and to explore the field of materials chemistry. The Fulbright Research Grant (2003) and the Kosciuszko Foundation Grant (2007) to IN for research in the USA are acknowledged. BASF (Poland & Belgium) and Companhia Brasilia de Metalurgia e Mineraçáo (CBMM, Brazil) are recognized for donating F127 copolymer and niobium source used in this study, respectively.

References

Bagshaw, S.A., Prouzet, E., Pinnavaia, T.J.: Science **269**, 1242 (1995)

Cheng, Ch.-F., Lin, Y.-Ch., Cheng, H.-H., Chen, H.-Ch.: Chem. Phys. Lett. **382**, 496 (2003)

Cheng, Ch.-F., Lin, Y.-Ch., Cheng, H.-H., Liu, Sh.-M., Sheu, H.-Sh.: Chem. Lett. **33**, 262 (2004)

Fulvio, P.E., Grabicka, B.E., Grudzien, R.M., Jaroniec, M.: Adsorp. Sci. Technol. **25**, 439 (2007)

Galarneau, A., Cambon, N., Di Renzo, F., Ryoo, R., Choi, M., Fajula, F.: New J. Chem. **27**, 73 (2003)

Grudzien, R.M., Grabicka, B.E., Jaroniec, M.: J. Mater. Chem. **16**, 819 (2006)

Grudzien, R.M., Grabicka, B.E., Jaroniec, M.: Appl. Surf. Sci. **253**, 5660 (2007)

Huo, Q., Margolese, D.I., Ciesla, U., Demuth, D.G., Feng, P., Gier, T.E., Sieger, P., Firouzi, A., Chmelka, B.F., Schuth, F., Stucky, G.D.: Chem. Mater. **6**, 1176 (1994)

Imperor-Clerc, M., Davidson, P., Davidson, A.: J. Am. Chem. Soc. **122**, 11925 (2000)

Jaroniec, M., Kruk, M., Olivier, J.P.: Langmuir **15**, 5410 (1999)

Kim, T.-W., Ryoo, R., Kruk, M., Gierszal, K.P., Jaroniec, M., Kamiya, S., Teresaki, O.: J. Phys. Chem. B **108**, 11480 (2004)

Kleitz, F., Solovyov, L.A., Anilkumar, G.M., Choi, S.H., Ryoo, R.: Chem. Commun. 1536 (2004)

Kresge, C.T., Leonowicz, M.E., Roth, W.J., Vartuli, J.C., Beck, J.S.: Nature **359**, 710 (1992)

Kruk , M., Jaroniec, M., Sayari, A.: Langmuir **13**, 6267 (1997)

Kruk, M., Jaroniec, M., Ko, C.H., Ryoo, R.: Chem. Mater. **12**, 1961 (2000)

Matos, J.R., Mercuri, L.P., Kruk, M., Jaroniec, M.: Langmuir **18**, 884 (2002)

Mesa, M., Sierra, L., Patarin, J., Guth, J.-L.: Solid State Sci. **7**, 990 (2005)

Nowak, I., Ziolek, M.: Microporous Mesoporous Mater. **78**, 281 (2005)

Nowak, I., Kasprzyk, B., Ziolek, M., Nawrocki, J.: Stud. Surf. Sci. Catal. **141**, 591 (2002)

Nowak, I., Kilos, B., Ziolek, M., Lewandowska, A.: Catal. Today **78**, 487 (2003)

Ravikovitch, P.I., Neimark, A.V.: Langmuir **18**, 1550 (2002)

Ryoo, R., Ko, C.H., Kruk , M., Antochshuk, V., Jaroniec, M.: J. Phys. Chem. B **104**, 11465 (2000)

Ryoo, R., Joo, S.H., Kruk, M., Jaroniec, M.: Adv. Mater. **13**, 677 (2001)

Sakamoto, Y., Kaneda, M., Terasaki, O., Zhao, D., Kim, J.M., Stucky, G.D., Shin, H.J., Ryoo, R.: Nature **449**, 408 (2000)

Ustinov, E.A., Do, D.D., Jaroniec, M.: J. Chem. Theory Comput. **1**, 653 (2005)

Van Der Voort, P., Benjelloun, M., Vansant, E.F.: J. Phys. Chem. B **106**, 9027 (2002)

Wang, L., Fan, J., Tian, B., Yang, H., Yu, Ch., Tu, B., Zhao, D.: Microporous Mesoporous Mater. **67**, 135 (2004)

Yamada, Y., Zhou, H.S., Uchida, H., Tomita, M., Ueno, Y., Honma, I., Asai, K., Katsube, T.: Microporous Mesoporous Mater. **54**, 269 (2002)

Yu, C., Yu, Y., Zhao, D.: Chem. Commun. 575 (2000)

Yu, C., Yu, Y., Miao, L., Zhao, D.: Microporous Mesoporous Mater. **44–45**, 65 (2001)

Zhang, W., Pinnavaia, T.J.: Catal. Lett. **38**, 261 (1996)

Zhao, D., Feng, J., Huo, Q., Melosh, N., Fredickson, G.H., Chmelka, B., Stucky, G.D.: Science **279**, 548 (1998a)

Zhao, D., Huo, Q., Feng, J., Chmelka, B.F., Stucky, G.D.: J. Am. Chem. Soc. **120**, 6024 (1998b)